J. Fluid Mech. (1978), *vol.* 84, *part* 4, *pp.* 769–793
Printed in Great Britain

Resonant interactions between topographic planetary waves in a continuously stratified fluid

By LAWRENCE A. MYSAK

National Center for Atmospheric Research, Boulder, Colorado 80307†

(Received 22 June 1977)

The resonant interactions between topographic planetary waves in a continuously stratified fluid are investigated theoretically. The interacting waves form a resonant triad and travel along a channel with a uniformly sloping bottom. The basic state stratification in the channel is characterized by a constant buoyancy frequency. The existence of solutions to the quadratic resonance conditions is established graphically. Each wave by itself is a bottom-intensified oscillation of the type discovered by Rhines (1970) except for the addition of a small positive frequency correction. This correction must be included to satisfy higher-order terms in the bottom boundary condition. For strong stratification ($r^2 \gg L^2$, where r = internal deformation radius and L = channel width), the waves are strongly bottom-trapped and this frequency correction is negligible. For weak stratification ($r^2 \ll L^2$) the waves are barotropic and the frequency correction is $O(\delta)$, where δ = fractional change in depth across the channel. In many oceanic contexts, δ lies in the range 0·1–0·4 and therefore this correction can produce a significant change in the phase speed. The amplitudes of the waves in the triad obey the classical gyroscopic equations usually encountered in quadratic resonance problems. In particular, the amplitudes evolve on the slow time scale

$$t = O(1/f_0 \delta^2),$$

which for our scaling assumptions is also $O(1/f_0 Ro)$, where Ro is the Rossby number.

The results are applied to the Norwegian continental slope region. It is shown that, in this vicinity, there may exist resonant triads consisting of two short, high-frequency waves (periods around 3–4 days) and one long, low-frequency wave (period around 9 days).

1. Introduction

Several investigators have recently suggested that the observed fluctuations of various ocean current systems flowing along steep bottom slopes may be due to baroclinic instability of the mean flow (Smith 1976; Mysak & Schott 1977; Mysak 1977; J. A. Helbig 1977, private communication). In each of these studies, the traditional theory (e.g. see Pedlosky 1964) of baroclinic instability of a channel flow along a uniform slope is applied in an attempt to explain the presence of current and temperature fluctuations which are characterized by periods of a few days and wavelengths

† Permanent address: Department of Mathematics and Institute of Oceanography, University of British Columbia, Vancouver, B.C. V6T 1W5.

of 100 km or less. In the development of this traditional theory, it is assumed that $Ro/\delta = O(1)$, where Ro denotes the Rossby number of the mean flow ($Ro = U/f_0 L$, where U = horizontal velocity scale, f_0 = mean value of the Coriolis parameter and L = channel width) and δ denotes the fractional change in depth across the channel ($\delta = \alpha L/H$, where α = bottom slope and H = characteristic channel depth). Physically the assumption $Ro/\delta = O(1)$ means that the destabilizing influence of the vertical shear can effectively compete with the possible stabilizing influence of the bottom slope. A second assumption in the traditional theory is that the wave restoring forces associated with topography and a variable Coriolis parameter are comparable. Third, it is assumed in the theory that the motions are characterized by the advective time scale L/U.

An examination of the velocity, time and length scales associated with the flows studied by the authors mentioned above reveals that the above three assumptions are not strictly valid. Thus there is some question as to whether the traditional theory of baroclinic instability is relevant in each of the situations considered. The flows studied in these papers (the Denmark Strait overflow, the Norwegian Current, the California Undercurrent and the Strait of Georgia mean current) are fairly weak and are of variable width; however, each is characterized by a Rossby number $Ro = O(10^{-2})$. For example, the California Undercurrent off Vancouver Island is characterized by $U = 20$ cm/s, $f_0 = 1{\cdot}1 \times 10^{-4}$ s^{-1} and $L = 50$ km, giving $Ro = 3{\cdot}6 \times 10^{-2}$. On the other hand, the bottom slope beneath each of these flows is relatively large, with α typically $O(10^{-2})$; the corresponding value of δ in each case is $O(10^{-1})$. For the California Undercurrent example referred to above, $\alpha = 1{\cdot}9 \times 10^{-2}$ and $H = 2500$ m, giving

$$\delta = 3{\cdot}8 \times 10^{-1}.$$

Therefore, in each of these regions $Ro/\delta = O(10^{-1})$, rather than $O(1)$ as assumed in the traditional theory. Physically speaking, this means that the destabilizing influence of vertical shear is dominated by the stabilizing influence of topography. Further, it is well known (LeBlond & Mysak 1978, chap. 3) that, when the bottom slope

$$\alpha = O(10^{-2}),$$

a sloping topography completely dominates the earth's curvature effect (the beta effect) as a restoring force for low-frequency wave motions. Hence, the second assumption of the traditional theory is invalid in each of these regions. Finally, for the weak flows considered, the advective time scale L/U typically corresponds to a period of several weeks to a few months, which is considerably longer than the periods observed (a few days). The observed temporal fluctuations in each case are more aptly characterized by the shorter time scale $1/f_0\delta$, which is the characteristic time scale for topographic planetary waves.

In summary, the motions in the different regions studied by the above authors are characterized by the parameter inequalities

$$Ro \ll \delta \ll 1 \tag{1.1}$$

and

$$(L/R)\cot\phi_0 \ll \delta, \tag{1.2}$$

where ϕ_0 = mean latitude and R = radius of the earth. The inequality (1.2) reflects the

dominating influence of topography over the beta effect. Moreover, it is noted that in the regions studied

$$Ro \sim (L/R)\cot\phi_0 = O(\delta^2). \tag{1.3}$$

This relation and (1.1) express the fact the nonlinearities are weak, and that the lowest-order flow will be linear and governed by topography. Further, a more realistic time scale for the motions is

$$t \sim 1/f_0\delta. \tag{1.4}$$

Finally, it is noted that the Burgers number is characteristically of order unity, namely

$$B = r^2/L^2 = O(1), \tag{1.5}$$

where r denotes the internal deformation radius.

In the traditional theory of baroclinic instability, as developed in Pedlosky (1964), only (1.5) holds. Otherwise, it is assumed that the appropriate time scale is the advective 'mesoscale' time L/U and that the following ordering applies:

$$Ro \sim (L/R)\cot\phi_0 \sim \delta \ll 1.$$

These considerations motivated the author to formulate the problem studied in this paper. It will be shown that the assumptions (1.1)–(1.5) naturally lead to the study of resonant interactions between topographic planetary waves in a stratified fluid. In such resonant interactions it is required that the nonlinearities be weak so that the waves involved are basically linear and have topography as their restoring force. Then the energy transfers between the waves will take place over a time that is long compared with the wave period. This will be the case if we choose our scaling to be consistent with the parameter ordering (1.2) and (1.3). In the theory of baroclinic instability with topography, on the other hand, the scales are chosen so that nonlinearities and topography are of equal importance. Then the energy transfers between the waves and the mean flow take place over a much shorter time scale, of the order of the wave period. To have a clear picture of the types of waves involved in these interactions, we now briefly discuss the lowest-order, non-trivial flow.

To the zeroth order in the expansion parameter δ, the wave motion discussed here is geostrophic and the geostrophic pressure $p^{(0)}$ satisfies a *linear* potential vorticity equation. For a channel with a uniform bottom slope containing a fluid with constant stratification (i.e. B = constant), this equation and the associated boundary conditions have the travelling-wave solution (Rhines 1970)

$$p_m^{(0)} = A_m \sin m\pi x \cos(ly - \omega_m t)\cosh K_m B^{\frac{1}{2}}(z-1) \tag{1.6}$$

with dispersion relation

$$\omega_m = lB^{\frac{1}{2}}/K_m \tanh K_m B^{\frac{1}{2}}, \tag{1.7}$$

where $K_m = (m^2\pi^2 + l^2)^{\frac{1}{2}}$ and m is a positive integer (see also §4). In (1.6) x and y (the cross-channel and long-channel co-ordinates) have been scaled by L, z (the vertical co-ordinate) by H, and t by $1/f_0\delta$ (see 1.4); $p^{(0)}$ has been scaled by $\rho_* LUf_0$ (ρ_* = constant reference density). In the limit $B \to 0$ (a homogeneous ocean), $p^{(0)}$ becomes independent of depth (the motion is barotropic) and (1.7) reduces to $\omega_m = l/K_m^2$, the familiar dispersion relation for a non-divergent topographic planetary wave. In the limit $B \to \infty$ (strong stratification) on the other hand, (1.5) implies that the motion is bottom intensified and the corresponding dispersion relation is $\omega_m = lB^{\frac{1}{2}}/K_m$, which

represents the frequency of a long period buoyancy oscillation. Under the assumption (1.3), the boundary-value problem for the first-order pressure $p^{(1)}$, where

$$p = p^{(0)} + \delta p^{(1)} + \ldots,$$

can be readily formulated. (We note here that p denotes the total pressure minus the static hydrostatic pressure.) It is the consideration of the boundary-value problem for $p^{(1)}$ that leads to the study of a resonant triad of waves, in which each wave is of the form (1.6) and has (1.7) (with a small correction added on) as the dispersion relation. However, the amplitude of each wave in this triad is now a function of the slow time variable $T = \delta t$. The novel feature about this resonant interaction problem is that the amplitude equations are derived by applying the usual closure condition (elimination of secular terms) to the bottom boundary condition for $p^{(1)}$. In most quadratic resonant interaction problems the closure condition is applied to the governing differential equation for the first-order field.

The study of resonantly interacting planetary waves on the beta plane has had a long history. The barotropic problem has been examined by Kenyon (1964), Longuet-Higgins & Gill (1967), Newell (1969) and Plumb (1977). The baroclinic case has been studied by Newell (1972), Loesch (1974), Pedlosky (1975), Richman (1976) and Loesch & Domaracki (1977). In all these planetary wave studies, however, the fluid is taken to be of constant depth. It appears that the subject of resonant interactions between topographic planetary waves (which is discussed here) has never been treated in the literature.

Despite the elegance of resonant interaction theories, tests of them in the ocean or in the laboratory are notoriously difficult to perform. To date, the most successful resonant interaction experiments have been performed in connexion with capillary, gravity and internal waves [see LeBlond & Mysak (1978, chap. 6), for a brief survey of these experiments]. There have been no reports of experiments that successfully identified resonant planetary wave triads in the ocean. Part of the problem may be that most of the earlier work has dealt only with interactions between discrete waves, whereas observations in the ocean suggest that energy transfers in the frequency (ω) and wavenumber (l) spectra occur continuously over a broad band of ω, l space. Thus it is conceivable that, if resonant interactions between topographic waves are to be observed in the ocean over steep bottom slopes, the theory described in this paper will have to be extended to the continuum case. In particular, the governing transport equation for the wave action spectrum will have to be integrated numerically.

The order of the presentation will be as follows. The governing equations of motion are introduced in §2, which is followed by the formulation of the boundary-value problems for the zeroth-order and first-order pressure fields $p^{(0)}$ and $p^{(1)}$ (§3). The solution for a single wave is then given in §4. We begin the analysis of a resonant triad of waves in §5, where graphical solutions to the resonance conditions are also given. The governing nonlinear differential equations for the slowly varying amplitudes of the resonant waves are derived in §6 and their qualitative behaviour is discussed in §7. Finally, in §8 the results are applied to the Norwegian Current.

2. Governing equations

We shall focus our attention on the quasi-geostrophic motions of a stably stratified, inviscid fluid lying in an infinitely long, variable-depth channel of arbitrary orientation (figure 1). The channel has vertical walls at $x = 0, L$, a rigid horizontal lid at $z = H$; the equation of the channel floor is given by $z = \delta H b(x)$. Here δ represents the fractional change in depth across the channel, a non-dimensional parameter which is assumed to be small. The function $b(x)$ describes the bottom profile and, being dimensionless, is assumed to be $O(1)$; also $b(0) = 0$. As an example, consider a channel of uniform bottom slope α. In this case

$$\delta = \alpha L/H \tag{2.1}$$

and

$$b(x) = x/L. \tag{2.2}$$

In many oceanic situations of interest, including those described in § 1, $L \gg H$ and therefore (2.1) implies that $\delta \gg \alpha$. However, because the bottom slope itself is usually very small, in these same situations δ is still considerably less than unity.

To describe the fluid motions in the channel, we begin with the following adiabatic equations:

horizontal momentum:

$$\frac{Du}{Dt} - fv + \frac{1}{\rho_*} p_x^T = 0, \tag{2.3a}$$

$$\frac{Dv}{Dt} + fu + \frac{1}{\rho_*} p_y^T = 0, \tag{2.3b}$$

hydrostatic:

$$p_z^T = -\rho^T g, \tag{2.4}$$

continuity:

$$\nabla . \mathbf{u} = 0, \tag{2.5}$$

incompressibility:

$$\frac{D\rho^T}{Dt} = 0, \tag{2.6}$$

where (u, v, w) are the velocity components in the (x, y, z) directions respectively, ρ_* is a constant reference density (the Boussinesq approximation has been made in (2.3)), p^T and ρ^T denote the total pressure and density respectively,

$$\frac{D}{Dt} = \frac{\partial}{\partial t} + u\frac{\partial}{\partial x} + v\frac{\partial}{\partial y} + w\frac{\partial}{\partial z} \tag{2.7}$$

and

$$f = f_0[1 + R^{-1} \cot \phi_0 (x \sin \nu + y \cos \nu)], \tag{2.8}$$

where $f_0 = 2\Omega \sin \phi_0$ is the value of the Coriolis parameter evaluated at the reference latitude ϕ_0 and R = radius of the earth. The condition of zero normal flow across the boundaries of the channel implies that

$$u = 0 \quad \text{at} \quad x = 0, L, \tag{2.9}$$

$$w = 0 \quad \text{at} \quad z = H, \tag{2.10}$$

$$w = \delta H u \frac{db}{dx} \quad \text{at} \quad z = \delta H b(x). \tag{2.11}$$

We now introduce the following non-dimensional dependent and independent variables (denoted by primes):

$$\left.\begin{aligned} x, y &= L(x', y'), \quad z = Hz', \quad t = (f_0 \delta)^{-1} t', \\ u, v &= U(u', v'), \quad w = (\delta HU/L) w', \\ p^T &= p_0(z) + (\rho_* f_0 LU) p', \quad \rho^T = \rho_0(z) + (\rho_* f_0 LU/gH) \rho', \end{aligned}\right\} \tag{2.12}$$

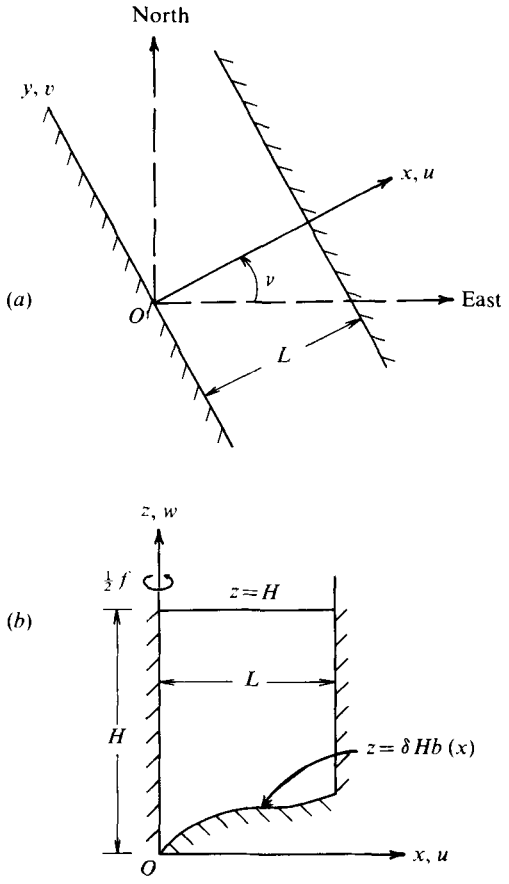

FIGURE 1. (*a*) Plan view and (*b*) cross-section of channel showing co-ordinate system and bottom topography. It is assumed that $0 < \delta \ll 1$ and $b(x) = O(1)$, $b(0) = 0$. The channel is situated on the beta plane and therefore the Coriolis parameter f varies linearly with latitude.

where U denotes a characteristic horizontal velocity and p_0, ρ_0 denote the basic state hydrostatic pressure and density, i.e. $dp_0/dz = -\rho_0 g$. Since the fluid is assumed to be stably stratified, the square of the buoyancy frequency is positive, namely

$$N^2(z) = -\frac{g}{\rho_*}\frac{d\rho_0}{dz} > 0. \tag{2.13}$$

The scales used in (2.12) are in keeping with those generally used in studies of quasi-geostrophic motions (Pedlosky 1964), except for our choice of the time scale, which reflects the dominating influence of topography over nonlinearity. Substituting (2.12) into (2.3)–(2.8) and then dropping the primes, we obtain the following system of equations:

$$\delta u_t + \delta^2\gamma(uu_x + vu_y + \delta wu_z) - [1 + \delta^2\beta(x\sin\nu + y\cos\nu)]\,v + p_x = 0, \tag{2.14}$$

$$\delta v_t + \delta^2\gamma(uv_x + vv_y + \delta wv_z) + [1 + \delta^2\beta(x\sin\nu + y\cos\nu)]\,u + p_y = 0, \tag{2.15}$$

$$p_z = -\rho, \tag{2.16}$$

$$u_x + v_y + \delta w_z = 0, \tag{2.17}$$

$$\rho_t + \delta\gamma(u\rho_x + v\rho_y + \delta w\rho_z) - B(z)\,w = 0, \tag{2.18}$$

where

$$\gamma = \frac{U/f_0 L}{\delta^2} \equiv \frac{Ro}{\delta^2}, \tag{2.19}$$

$$\beta = \frac{(L/R)\cot\phi_0}{\delta^2}, \tag{2.20}$$

$$B(z) = \frac{N^2(z)H^2/f_0^2}{L^2} \equiv \frac{r^2}{L^2} \tag{2.21}$$

denote respectively the inertial factor, the planetary vorticity factor and the Burgers number. In (2.19) and (2.21) we have also introduced the familiar Rossby number, Ro, and the internal deformation radius, r. The non-dimensional forms of the boundary conditions (2.9)–(2.11) are

$$u = 0 \quad \text{at} \quad x = 0, 1, \tag{2.22}$$

$$w = 0 \quad \text{at} \quad z = 1, \tag{2.23}$$

$$w = u\frac{db}{dx} \quad \text{at} \quad z = \delta b. \tag{2.24a}$$

We wish to emphasize here that, in (2.24a), b is written in terms of the non-dimensional cross-channel co-ordinate. Thus for the linearly varying bottom profile (2.2), b in (2.24a) takes the simple form $b = x$.

In accordance with (1.3) and (1.5) we shall assume that γ, β and $B(z)$ are each of order unity. Thus (2.14)–(2.24a) contain only one small parameter, $\delta = O(10^{-1})$, a fact which we shall exploit in § 3. However, before proceeding to the next section, we first expand the bottom boundary condition (2.24a) in a Taylor series about $z = 0$:

$$w + w_z\,\delta b = (u + u_z\,\delta b)\frac{db}{dx} + O(\delta^2) \quad \text{at} \quad z = 0. \tag{2.24b}$$

3. Asymptotic solution of governing equations

To avoid the occurrence of secular terms in the subsequent analysis, we now allow each dependent variable to depend on two time variables, a 'fast' time t and a 'slow' time T, the latter being defined by

$$T = \delta t. \tag{3.1}$$

Thus $Q = Q(x, y, z, t, T)$, where Q stands for any of the dependent variables. Accordingly, the time derivative in the non-dimensional equations (2.14)–(2.18) transforms as

$$\partial_t \to \partial_t + \delta\partial_T. \tag{3.2}$$

We shall see later (§ 6) that the amplitudes of resonantly interacting waves will evolve on the slow time scale T.

We now assume that each dependent variable has an asymptotic expansion of the form

$$Q \sim Q^{(0)} + \delta Q^{(1)} + \delta^2 Q^{(2)} + \ldots \quad \text{as} \quad \delta \to 0. \tag{3.3}$$

The substitution of (3.2) and (3.3) into (2.14)–(2.18) and the boundary conditions (2.22), (2.23) and (2.24b) then yields a hierarchy of equations. To $O(\delta^0)$ we obtain the geostrophic equations

$$-v^{(0)} + p_x^{(0)} = 0, \tag{3.4a}$$

$$u^{(0)} + p_y^{(0)} = 0, \tag{3.4b}$$

$$p_z^{(0)} = -\rho^{(0)}, \tag{3.5}$$

$$u_x^{(0)} + v_y^{(0)} = 0, \tag{3.6}$$

$$\rho_t^{(0)} - Bw^{(0)} = 0, \tag{3.7}$$

with boundary conditions

$$u^{(0)} = 0 \quad \text{at} \quad x = 0, 1, \tag{3.8}$$

$$w^{(0)} = 0 \quad \text{at} \quad z = 1, \tag{3.9}$$

$$w^{(0)} = u^{(0)}\frac{db}{dx} \quad \text{at} \quad z = 0. \tag{3.10}$$

The $O(\delta)$ equations and boundary conditions are

$$u_t^{(0)} - v^{(1)} + p_x^{(1)} = 0, \tag{3.11a}$$

$$v_t^{(0)} + u^{(1)} + p_y^{(1)} = 0, \tag{3.11b}$$

$$p_z^{(1)} = -\rho^{(1)}, \tag{3.12}$$

$$u_x^{(1)} + v_y^{(1)} + w_z^{(0)} = 0, \tag{3.13}$$

$$\rho_t^{(1)} + \rho_T^{(0)} + \gamma(u^{(0)}\rho_x^{(0)} + v^{(0)}\rho_y^{(0)}) - Bw^{(1)} = 0, \tag{3.14}$$

$$u^{(1)} = 0 \quad \text{at} \quad x = 0, 1, \tag{3.15}$$

$$w^{(1)} = 0 \quad \text{at} \quad z = 1, \tag{3.16}$$

$$w^{(1)} + w_z^{(0)}b = (u^{(1)} + u_z^{(0)}b)\frac{db}{dx} \quad \text{at} \quad z = 0. \tag{3.17}$$

Of the $O(\delta^2)$ equations and boundary conditions, all that will be needed for our purposes here are the second-order horizontal momentum and continuity equations:

$$u_t^{(1)} + u_T^{(0)} + \gamma(u^{(0)}u_x^{(0)} + v^{(0)}u_y^{(0)}) - v^{(2)} - (\beta_1 y + \beta_2 x)\, v^{(0)} + p_x^{(2)} = 0, \tag{3.18a}$$

$$v_t^{(1)} + v_T^{(0)} + \gamma(u^{(0)}v_x^{(0)} + v^{(0)}v_y^{(0)}) + u^{(2)} + (\beta_1 y + \beta_2 x)\, u^{(0)} + p_y^{(2)} = 0, \tag{3.18b}$$

$$u_x^{(2)} + v_y^{(2)} + w_z^{(1)} = 0, \tag{3.19}$$

where

$$\beta_1 = \beta\cos\nu, \quad \beta_2 = \beta\sin\nu. \tag{3.20}$$

We now derive the vorticity balance equations for $p^{(0)}$ (the geostrophic pressure) and $p^{(1)}$. Since $p^{(0)}$ behaves like a stream function, (3.6) is redundant and the zeroth-order problem is indeterminate. The equation for $p^{(0)}$ is therefore obtained by cross-differentiating (3.11), the first-order momentum equations, and then eliminating all the variables in favour of $p^{(0)}$ by employing (3.4), (3.5), (3.7) and (3.13). The result is

$$[\nabla^2 p^{(0)} + (B^{-1}p_z^{(0)})_z]_t = 0, \tag{3.21}$$

where $\nabla^2 = \partial_{xx} + \partial_{yy}$. Equation (3.21) expresses the fact that (the lowest-order) potential vorticity is conserved. Because of our scaling assumptions, (3.21) is linear and the potential vorticity consists of only the relative vorticity part (first term) and the interior vortex stretching part. Integrating (3.21) with respect to t and setting the function of integration equal to zero gives

$$\nabla^2 p^{(0)} + (B^{-1}p_z^{(0)})_z = 0. \tag{3.22}$$

Equation (3.22) holds only if there are no sources or sinks of vorticity, a condition which we shall assume throughout the remainder of this paper. Using (3.4b), (3.5) and (3.7), the boundary conditions (3.8)–(3.10) take the form

$$p_{zt}^{(0)} = 0 \quad \text{at} \quad x = 0, 1, \tag{3.23}$$

$$p_{zt}^{(0)} = 0 \quad \text{at} \quad z = 1, \tag{3.24}$$

$$B^{-1}p_{zt}^{(0)} - p_y^{(0)}\frac{db}{dx} = 0 \quad \text{at} \quad z = 0. \tag{3.25}$$

The equation for $p^{(1)}$ is obtained by first cross-differentiating (3.18) to eliminate $p^{(2)}$; a lengthy series of substitutions involving (3.19) and the lower-order equations finally yields

$$[\nabla^2 p^{(1)} + (B^{-1}p_z^{(1)})_z]_t = \beta_2 p_y^{(0)} - \beta_1 p_x^{(0)} - [\nabla^2 p^{(0)} + (B^{-1}p_z^{(0)})_z]_T + \gamma J[\nabla^2 p^{(0)} + (B^{-1}p_z^{(0)})_z, p^{(0)}], \quad (3.26)$$

where $J(f,g) = f_x g_y - f_y g_x$ denotes the Jacobian operator. Because we have taken (3.22) as the governing equation for $p^{(0)}$, the last two terms on the right-hand side of (3.26) drop out and we are left with

$$[\nabla^2 p^{(1)} + (B^{-1}p_z^{(1)})_z]_t = \beta_2 p_y^{(0)} - \beta_1 p_x^{(0)}. \quad (3.27)$$

The boundary conditions (3.15)–(3.17) become

$$p_y^{(1)} = -p_{xt}^{(0)} \quad \text{at} \quad x = 0, 1, \quad (3.28)$$

$$p_{zt}^{(1)} = -p_{zT}^{(0)} - \gamma J(p^{(0)}, p_z^{(0)}) \quad \text{at} \quad z = 1, \quad (3.29)$$

$$B^{-1}p_{xt}^{(1)} - p_y^{(1)}\frac{db}{dx} = -B^{-1}p_{zT}^{(0)} - B^{-1}\gamma J(p^{(0)}, p_z^{(0)}) + p_{xt}^{(0)}\frac{db}{dx} - \left[\left(B^{-1}p_{zt}^{(0)} - p_y^{(0)}\frac{db}{dx}\right)_z\right] b \quad \text{at} \quad z = 0. \quad (3.30)$$

In the subsequent sections we shall discuss the travelling-wave solutions of the above systems of equations for $p^{(0)}$ and $p^{(1)}$. First, in §4, we shall determine the single-wave solution for $p^{(0)}$ and its correction $p^{(1)}$ and second, in §§5–8, we shall study the behaviour of a resonant triad of waves. We mentioned earlier that it is the boundary-value problem for $p^{(1)}$ that is important for the resonant wave triad study. This is because it is from the bottom boundary condition for $p^{(1)}$ that we get the amplitude equations that describe the slow time evolution of the wave triad. We do not need the solution for $p^{(1)}$ itself for the resonant triad study, but we include it here for the sake of completeness. We find, for example, that $p^{(1)}$ has components both in phase and in quadrature with $p^{(0)}$.

4. Single-wave solution

We now suppose that B = constant (i.e. N = constant) and that the channel has a uniform bottom slope, so that $b = x$ (see sentences following (2.24a)). Then travelling-wave solutions of (3.22)–(3.25) can be readily written down in terms of elementary functions. The solution for a single wave corresponding to a given cross-channel mode m has the form

$$p^{(0)} = A_m(T)\sin m\pi x \cosh K_m B^{\frac{1}{2}}(z-1)\exp[i(ly - \omega_m t)], \quad (4.1)$$

where $K_m = (m^2\pi^2 + l^2)^{\frac{1}{2}}$, $m = 1, 2, \ldots$, and ω_m and l are related through

$$\omega_m = l B^{\frac{1}{2}}/K_m \tanh K_m B^{\frac{1}{2}}. \quad (4.2)$$

The amplitude function $A_m(T)$ will be determined at the next order. Without loss of generality, we take $l > 0$ so that (4.2) implies that $\omega_m > 0$; thus the phase of the wave travels in the positive y direction (see (4.1)). Examples of the dispersion curves for different modes are plotted in figure 2. Note that for sufficiently small B (weak

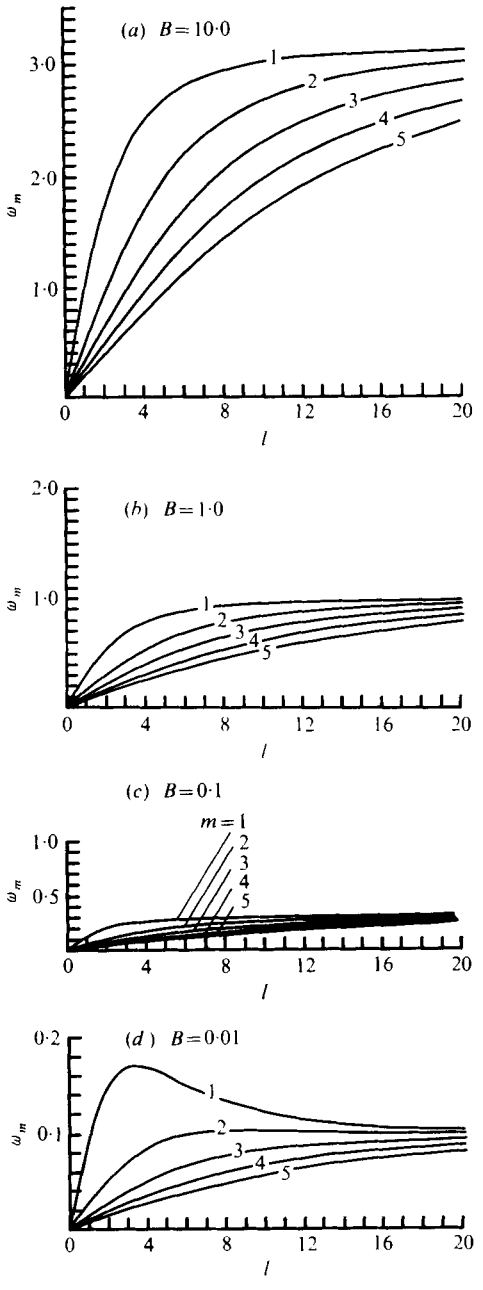

FIGURE 2. Dispersion curves as given by (4.2) for the first five cross-channel modes ($m = 1, \ldots, 5$, the numbers on the curves) for various values of the Burgers number $B = r^2/L^2$, where r = internal deformation radius and L = channel width. ω_m = frequency and l = wavenumber. Note that the vertical scale in (*d*) has been magnified about tenfold.

stratification), the dispersion curve for a given mode m has a zero slope at some intermediate value of $k = k_0$ and hence the group velocity $c_g < 0$ for $k > k_0$. That is, the energy of the very short waves in a weakly stratified fluid propagates in the *negative y* direction, in opposition to the phase velocity.

For the case of weak stratification ($B \ll 1$), (4.1) and (4.2) reduce to the barotropic topographic planetary wave solution:

$$p^{(0)} = A_m(T)\sin m\pi x \exp[i(ly - \omega_m t)],$$
$$\omega_m = l/K_m^2. \tag{4.3}$$

For strong stratification ($B \gg 1$) on the other hand, the motion is bottom intensified:

$$p^{(0)} = \tfrac{1}{2}A_m(T)\sin m\pi x \exp[KB^{\frac{1}{2}}(1-z) + i(ly - \omega_m t)]. \tag{4.4}$$

In this limit, the dispersion relation takes the form

$$\omega_m = lB^{\frac{1}{2}}/K_m. \tag{4.5}$$

Convincing observational evidence of these bottom-trapped waves in the ocean, first predicted theoretically by Rhines (1970), has only recently been presented (Thompson & Luyten 1976).

The solution of (3.27)–(3.30) in which B = constant, $b = x$ and $p^{(0)}$ is given by (4.1) is not trivial. Substitution of $p^{(0)}$ into (3.27)–(3.30) (with B = constant, $b = x$) yields

$$\nabla^2 p_t^{(1)} + B^{-1}p_{zzt}^{(1)} = A_m(\beta_2 il\sin m\pi x - \beta_1 m\pi\cos m\pi x)\cosh K_m B^{\frac{1}{2}}(z-1)\exp(i\theta_m), \tag{4.6}$$

$$p_y^{(1)} = i\omega_m A_m m\pi\cos m\pi x\cosh K_m B^{\frac{1}{2}}(z-1)\exp(i\theta_m) \quad \text{at} \quad x = 0, 1, \tag{4.7}$$

$$p_{zt}^{(1)} = 0 \quad \text{at} \quad z = 1, \tag{4.8}$$

$$B^{-1}p_{zt}^{(1)} - p_y^{(1)} = (K_m/B^{\frac{1}{2}})\sinh K_m B^{\frac{1}{2}}\sin m\pi x\exp(i\theta_m)\frac{dA_m}{dT}$$
$$- i\omega_m m\pi\cosh K_m B^{\frac{1}{2}}\cos m\pi x\exp(i\theta_m)A_m$$
$$+ i(lK_m B^{\frac{1}{2}}/\sinh K_m B^{\frac{1}{2}})x\sin m\pi x\exp(i\theta_m)A_m \quad \text{at} \quad z = 0, \tag{4.9}$$

where for short

$$\theta_m = ly - \omega_m t. \tag{4.10}$$

We write the solution for $p^{(1)}$ in the form

$$p^{(1)} = p_{pa}^{(1)} + p_{ho}^{(1)}, \tag{4.11}$$

where

$$p_{pa}^{(1)} = \left(\frac{\beta_2 l}{2m\pi}x\cos m\pi x - \frac{i\beta_1}{2}x\sin m\pi x\right)(A_m/\omega_m)\cosh K_m B^{\frac{1}{2}}(z-1)\exp(i\theta_m)$$
$$= \left(\frac{\beta_2 l}{2m\pi}\sum_{n=1}^{\infty}a_n\sin n\pi x - \frac{i\beta_1}{2}x\sin m\pi x\right)(A_m/\omega_m)\cosh K_m B^{\frac{1}{2}}(z-1)\exp(i\theta_m), \tag{4.12}$$

in which

$$a_n = \begin{cases} -\tfrac{1}{2}m\pi & \text{for} \quad n = m, \\ -2n/\pi(n^2 - m^2) & \text{for} \quad n+m \quad \text{even}, \\ 2n/\pi(n^2 - m^2) & \text{for} \quad n+m \quad \text{odd}. \end{cases}$$

Clearly $p_{pa}^{(1)}$ is a particular solution to (4.6) which satisfies $\partial p^{(1)}/\partial y = 0$ at $x = 0$, 1, the boundary condition (4.8), and $B^{-1}p_{zt}^{(1)} - p_y^{(1)} = 0$ at $z = 0$. The function $p_{ho}^{(1)}$ represents a

homogeneous solution of (4.6) which is chosen to satisfy (4.8) and the inhomogeneous forms of (4.7) and (4.9). A suitable form for $p_{ho}^{(1)}$ is

$$p_{ho}^{(1)} = A_m(\omega_m m\pi/l)\cos m\pi x \cosh K_m B^{\frac{1}{2}}(z-1)\exp(i\theta_m) + A_m \exp(i\theta_m)\sum_{\substack{n=1\\ n\neq m}}^{\infty} b_n \sin n\pi x \cosh K_n B^{\frac{1}{2}}(z-1), \tag{4.13}$$

where $K_n = (n^2\pi^2 + l^2)^{\frac{1}{2}}$. The solution (4.13) clearly satisfies (4.6) with the right-hand side equal to zero and the boundary conditions (4.7), (4.8). The coefficients b_n in (4.13) are determined by substituting $p_{ho}^{(1)}$ into (4.9) in which $\cos m\pi x$ and $x\sin m\pi x$ are first expanded in terms of Fourier sine series; the result of these substitutions is

$$\begin{aligned} iA_m \sum_{\substack{n=1\\ n\neq m}}^{\infty} b_n[(K_n\omega_m/B^{\frac{1}{2}})\sinh K_n B^{\frac{1}{2}} - l\cosh K_n B^{\frac{1}{2}}]\sin n\pi x \\ = (K_m/B^{\frac{1}{2}})\sinh K_m B^{\frac{1}{2}} \sin m\pi x \frac{dA_m}{dT} \\ - i\omega_m m\pi \cosh K_m B^{\frac{1}{2}} A_m \sum_{n=1}^{\infty} c_n \sin n\pi x \\ + i(lK_m B^{\frac{1}{2}}/\sinh K_m B^{\frac{1}{2}})A_m \sum_{n=1}^{\infty} d_n \sin n\pi x, \end{aligned} \tag{4.14}$$

where

$$\begin{aligned} c_n &= 0 \quad \text{for} \quad n = m, \\ &= 0 \quad \text{for} \quad n+m \quad \text{even}, \\ &= 4n/\pi(n^2-m^2) \quad \text{for} \quad n+m \quad \text{odd}, \\ d_n &= \tfrac{1}{2} \quad \text{for} \quad n = m, \\ &= 0 \quad \text{for} \quad n+m \quad \text{even}, \\ &= -8mn/\pi^2(m^2-n^2)^2 \quad \text{for} \quad n+m \quad \text{odd}. \end{aligned}$$

Upon equating the nth term on the left-hand side of (4.14) to those with subscript n on the right-hand side we find

$$b_n = \frac{d_n K_m B^{\frac{1}{2}}/\sinh K_m B^{\frac{1}{2}} - c_n \omega_m m\pi \cosh K_m B^{\frac{1}{2}}}{(K_n\omega_m/B^{\frac{1}{2}})\sinh K_n B^{\frac{1}{2}} - l\cosh K_n B^{\frac{1}{2}}}, \quad n \neq m, \tag{4.15}$$

which, we note, is real. Upon equating to zero the terms with subscript m on the right-hand side of (4.14) we obtain

$$\frac{dA_m}{dT} = -\frac{ilB}{2\sinh^2 K_m B^{\frac{1}{2}}} A_m \tag{4.16}$$

as the differential equation for A_m. Equation (4.16) implies that

$$A_m = A_{m0}\exp(-i\omega_{m0}T), \tag{4.17}$$

where A_{m0} = constant and

$$\omega_{m0} = lB/2\sinh^2 K_m B^{\frac{1}{2}} > 0. \tag{4.18}$$

Combining (4.17) with (4.1) we obtain

$$p^{(0)} = A_{m0}\sin m\pi x \cosh K_m B^{\frac{1}{2}}(z-1)\exp\{i[ly - (\omega_m + \delta\omega_{m0})t]\}. \tag{4.19}$$

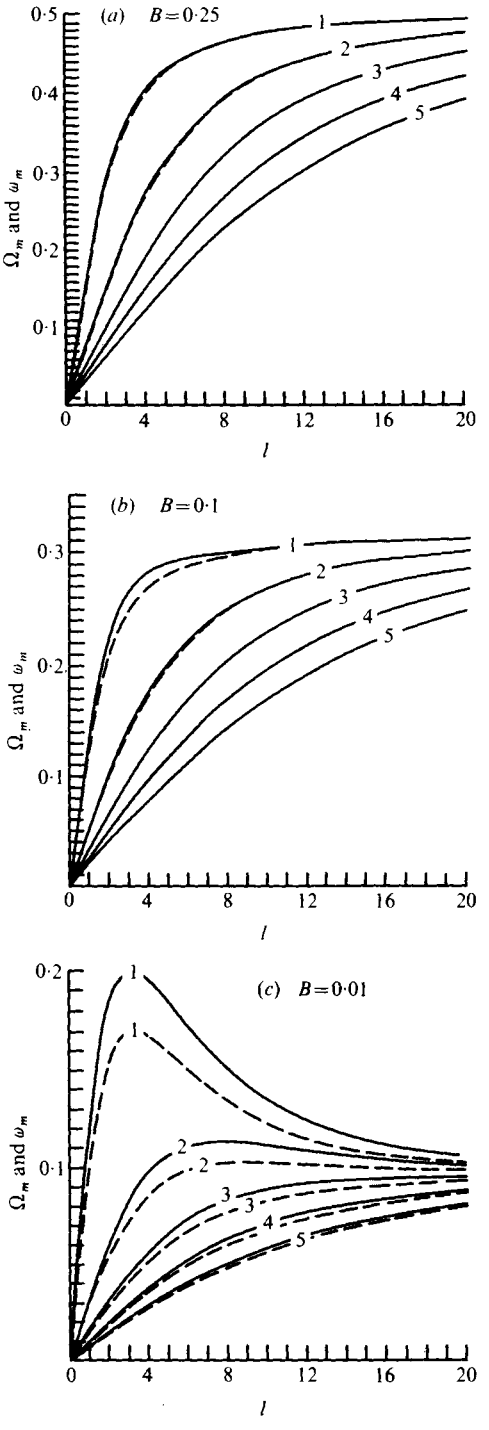

FIGURE 3. The corrected dispersion curves $\Omega_m(l)$ (solid lines), as given by (4.22), compared with the classical curves $\omega_m(l)$ (dashed lines), as given by (4.2), for various values of B. Ω_m and ω_m = frequency and l = wavenumber. In all cases, $\delta = 0{\cdot}4$. For $B = 10$ and 1 (the values also used in figure 2), the curves $\Omega_m(l)$ and $\omega_m(l)$ are essentially identical on the scales shown and therefore have not been plotted.

Thus we conclude that the lowest-order solution found by Rhines (1970) must contain a positive frequency correction in order to satisfy the next-order terms in the bottom boundary condition. Note that the phase speed of the wave is now given by

$$c_m = (\omega_m + \delta\omega_{m0})/l = \frac{B^{\frac{1}{2}}}{K_m \tanh K_m B^{\frac{1}{2}}} + \delta \frac{B}{2\sinh^2 K_m B^{\frac{1}{2}}}, \tag{4.20}$$

which is always larger than the 'classical value' given by ω_m/l. For bottom-trapped waves ($B \gg 1$), the correction is exponentially small; for barotropic waves however ($B \ll 1$), (4.20) gives the remarkably simple expression

$$c_m = (1/K_m^2)(1 + \tfrac{1}{2}\delta). \tag{4.21}$$

The corrected dispersion relation $\Omega_m(l)$, defined as

$$\Omega_m(l) \equiv \omega_m + \delta\omega_{m0} = \frac{l B^{\frac{1}{2}}}{K_m \tanh K_m B^{\frac{1}{2}}} + \frac{lB}{2\sinh^2 K_m B^{\frac{1}{2}}}, \tag{4.22}$$

is plotted in figure 3 for the case $\delta = 0{\cdot}4$. As expected from (4.22), the difference between $\Omega_m(l)$ and $\omega_m(l)$ increases as B decreases in figure 3. In particular, for very small B ($\leqslant O(10^{-2})$), the correction term gives a frequency increase of about 20% (figure 3*c*).

Upon combining (4.11), (4.12), (4.13), (4.15), and (4.17) we note that $p^{(1)}$ is also proportional to $\exp(-i\omega_{m0}\delta t)$ and hence that the correction $p^{(1)}$ also travels with phase speed (4.20). Further we note that all the terms in $p^{(1)}$ are in phase with $p^{(0)}$ except for the term proportional to β_1, which is in quadrature with $p^{(0)}$. For a north–south channel, however, this β_1 term drops out (see (3.20) with $\nu = \frac{1}{2}\pi$).

5. Resonant interactions

In §4 we found that the higher-order terms in the bottom boundary condition produced an $O(\delta)$ frequency correction in the lowest-order single-wave solution $p^{(0)}$. We now consider the energy exchanges between a resonant triad of such (frequency corrected) waves, written in real form. Thus we shall be concerned with describing the evolution of the wave combination

$$p^{(0)} = \sum_{q=1}^{3} A_{m_q}(T) \sin m_q \pi x \cosh K_{m_q} B^{\frac{1}{2}}(z-1) \exp[i(\theta_{m_q} - \omega_{m_q 0} T)] + \text{c.c. (complex conjugate)}, \tag{5.1}$$

where $\theta_{m_q} = l_q y - \omega_{m_q}(l_q)t$ and $\omega_{m_q}(l_q)$ and $\omega_{m_q 0}(l_q)$ are given by (4.2) and (4.18) respectively. For notational convenience we write (5.1) in the following, less cumbersome form:

$$p^{(0)} = \sum_{q=1}^{3} A_q(T) \sin m_q \pi x \cosh K_q B^{\frac{1}{2}}(z-1) \exp(i\Theta_q) + \text{c.c.}, \tag{5.2}$$

where $K_q = (l_q^2 + m_q^2 \pi^2)^{\frac{1}{2}}$, $\Theta_q = l_q y - \Omega_{m_q}(l_q)t$ and

$$\Omega_{m_q}(l_q) = \frac{l_q B^{\frac{1}{2}}}{K_q \tanh K_q B^{\frac{1}{2}}} + \delta \frac{l_q B}{2\sinh^2 K_q B^{\frac{1}{2}}}. \tag{5.3}$$

The combination (5.2) represents a resonant triad of waves (m_1, l_1, Ω_{m_1}), (m_2, l_2, Ω_{m_2}),

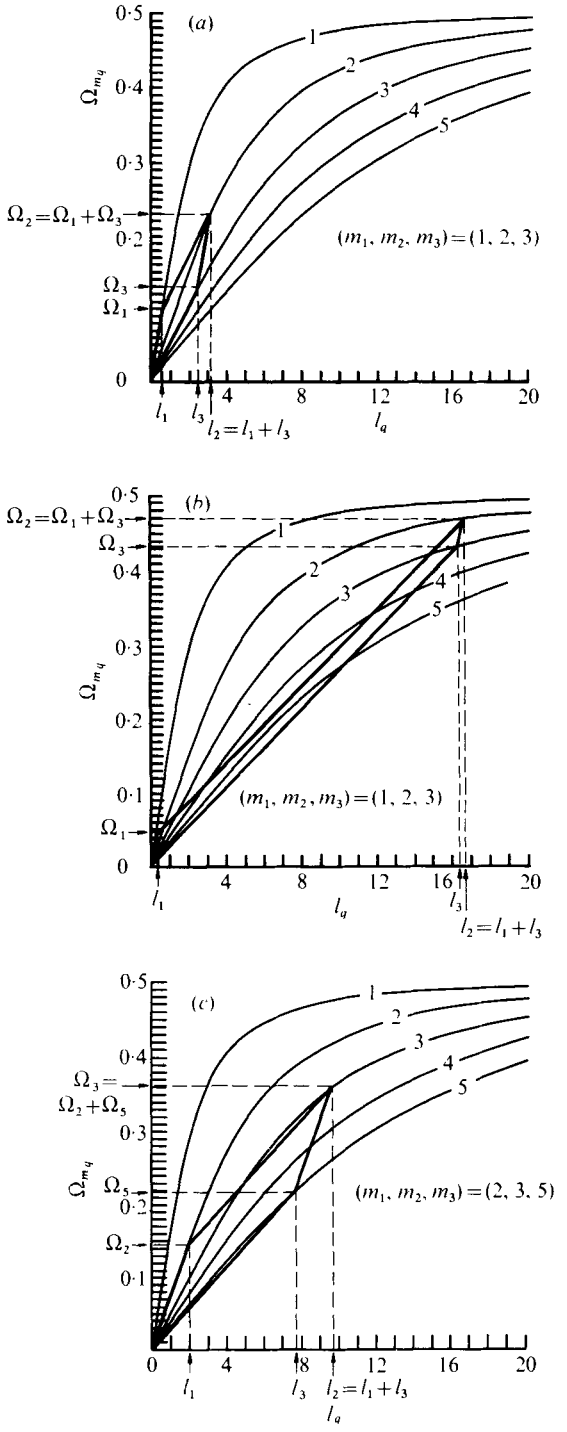

FIGURE 4. Examples of graphical solutions to the resonance conditions (5.5*b*). In each part $B = 0{\cdot}25$ and $\delta = 0{\cdot}4$. Ω_{m_q} = frequency and l_q = wavenumber.

(m_3, l_3, Ω_{m_3}) provided that the usual kinematic resonance conditions are satisfied:

$$\left.\begin{aligned}\Theta_1 \pm \Theta_2 \pm \Theta_3 &= 0,\\ m_1 \pm m_2 \pm m_3 &= 0.\end{aligned}\right\} \tag{5.4}$$

For definiteness, we shall consistently use the following form of (5.4) in conjunction with the resonant triad (5.1) or (5.2):

$$\left.\begin{aligned}\Theta_1 + \Theta_3 &= \Theta_2,\\ m_1 - m_3 &= -m_2,\end{aligned}\right\} \tag{5.5a}$$

or equivalently

$$\left.\begin{aligned}l_1 + l_3 &= l_2,\\ \Omega_{m_1} + \Omega_{m_3} &= \Omega_{m_2},\\ m_1 - m_3 &= -m_2,\end{aligned}\right\} \tag{5.5b}$$

where $l_q > 0$, $\Omega_{m_q} > 0$ and $m_q > 0$, $q = 1, 2, 3$. The equations for the amplitude functions $A_q(T)$ will be derived in the next section. Here we now show that the solution of (5.5*b*) can readily be obtained graphically from plots of the dispersion relation (5.3).

Figure 4 (*a*) shows the solution of (5.5*b*) for a triad of long waves. Since the waves are non-dispersive for small l ((5.3) implies that $\Omega_m \propto l$ as $l \to 0$), an infinity of parallelograms representing resonant triads can be constructed in the lower left corner of the Ω_m, l plane. Figure 4(*b*) shows the solution of (5.5*b*) also for the case $(m_1, m_2, m_3) = (1, 2, 3)$, but for waves of very different lengths [one long (l_1) and two short (l_2 and l_3) waves]. Finally, an example of a resonant triad consisting of higher-order cross-channel modes is shown in figure 4(*c*).

It is important to note here that there is no one favoured resonant triad or one favoured discrete set of resonant triads dictated by the dispersion relation. In view of the continuum of triads possible, expecially at long wavelengths, it would be of interest to look at the evolution of the wave action spectrum to see whether, for example, there is a continuous transfer of energy to the longer waves.

6. The amplitude equations

The equations for $A_q(T)$ are obtained by substituting the triad (5.1) into the right-hand side of the bottom boundary condition (3.30) (in which $b = x$) and then applying the resonance conditions (5.5). The first step yields, after much tedious algebra,

$$\begin{aligned}B^{-1}p_{xt}^{(1)} - p_y^{(1)} = {}& \frac{1}{B^{\frac{1}{2}}}\sum_{q=1}^{3} K_q \sinh K_q B^{\frac{1}{2}} \frac{dA_q}{dT} \exp(i\Theta_q) \sin m_q \pi x + \text{c.c.}\\ & - \frac{i}{B^{\frac{1}{2}}}\sum_{q=1}^{3} \omega_{m_q 0} K_q \sinh K_q B^{\frac{1}{2}} A_q \exp(i\Theta_q) \sin m_q \pi x + \text{c.c.}\\ & - \frac{\gamma\pi i}{2B^{\frac{1}{2}}}\sum_{1,2,3} P_{23} A_2 A_3 \exp[i(\Theta_2 + \Theta_3)][(l_2 m_3 - l_3 m_2)\sin(m_2 + m_3)\pi x\\ & + (l_2 m_3 + l_3 m_2)\sin(m_2 - m_3)\pi x] + \text{c.c.}\\ & - \frac{\gamma\pi i}{2B^{\frac{1}{2}}}\sum_{1,2,3} P_{23} A_2 A_3^* \exp[i(\Theta_2 - \Theta_3)][(l_2 m_3 + l_3 m_2)\sin(m_2 + m_3)\pi x\\ & + (l_2 m_3 - l_3 m_2)\sin(m_2 - m_3)\pi x] + \text{c.c.}\\ & - i\pi \sum_{q=1}^{3}\left(A_q \omega_{m_q} m_q \exp[i\Theta_q] \cosh K_q B^{\frac{1}{2}} \sum_{n=1}^{\infty} c_n^q \sin n\pi x\right) + \text{c.c.}\\ & + iB^{\frac{1}{2}} \sum_{q=1}^{3}\left(\frac{A_q l_q K_q}{\sinh K_q B^{\frac{1}{2}}} \exp[i\Theta_q] \sum_{n=1}^{\infty} d_n^q \sin n\pi x\right) + \text{c.c.},\end{aligned} \tag{6.1}$$

where

$$P_{jk} = -P_{kj} = (\cosh K_j B^{\frac{1}{2}})\, K_k \sinh K_k B^{\frac{1}{2}} - (\cosh K_k B^{\frac{1}{2}})\, K_j \sinh K_j B^{\frac{1}{2}}, \tag{6.2}$$

and

$$\left.\begin{aligned} c_n^q &= 0 \quad \text{for} \quad n = m_q, \\ &= 0 \quad \text{for} \quad n + m_q \quad \text{even}, \\ &= 4n/\pi(n^2 - m_q^2) \quad \text{for} \quad n + m_q \quad \text{odd}, \end{aligned}\right\} \tag{6.3}$$

$$\left.\begin{aligned} d_n^q &= \tfrac{1}{2} \quad \text{for} \quad n = m_q, \\ &= 0 \quad \text{for} \quad n + m_q \quad \text{even}, \\ &= -8m_q n/\pi^2(m_q^2 - n^2)^2 \quad \text{for} \quad n + m_q \quad \text{odd}. \end{aligned}\right\} \tag{6.4}$$

The symbol $\sum_{1,2,3}$ represents cyclic summation:

$$\sum_{1,2,3} a_2 a_3 \equiv a_2 a_3 + a_3 a_1 + a_1 a_2.$$

By balancing terms in the first summation and the cyclic summations in (6.1) according to (5.5a) we readily obtain the following equations for A_q:

$$\left.\begin{aligned} K_1 \sinh K_1 B^{\frac{1}{2}} \frac{dA_1}{dT} &= -isP_{23} A_2 A_3^*, \\ K_2 \sinh K_2 B^{\frac{1}{2}} \frac{dA_2}{dT} &= is P_{31} A_3 A_1, \\ K_3 \sinh K_3 B^{\frac{1}{2}} \frac{dA_3}{dT} &= -is P_{12} A_1^* A_2, \end{aligned}\right\} \tag{6.5}$$

where

$$0 < s = \tfrac{1}{2}\gamma\pi(l_2 m_3 - l_3 m_2) = \tfrac{1}{2}\gamma\pi(l_3 m_1 + l_1 m_3) = \tfrac{1}{2}\gamma\pi(l_1 m_2 + l_2 m_1). \tag{6.6}$$

It is important to note that these very simple equations are obtained because we choose $\Theta_1 + \Theta_3 = \Theta_2$ as part of the resonance conditions. If instead we used $\theta_1 + \theta_3 = \theta_2$ (which involves the uncorrected frequencies ω_m), each equation for A_q would also contain an extra term proportional to A_q. Also, it follows from (6.5) that, in terms of dimensional scales, the interaction time associated with (6.5) is $t = O(1/f_0\delta^2) = O(1/f_0 Ro)$ in view of the fact that we chose $\gamma = Ro/\delta^2 = O(1)$.

We note that, since $d_{m_q}^q = \frac{1}{2}$ and $\omega_{m_q 0}$ is given by (4.18), the terms in the second summation in (6.1) precisely cancel the three $d_{m_q}^q$ terms in the last summation. The remaining terms on the right-hand side of (6.1) give rise to a forced, non-resonant wave solution $p^{(1)}$ which will be $O(1)$ and therefore $\delta p^{(1)}$ will be small compared with the resonant triad $p^{(0)}$. The forced solution for $p^{(1)}$ can be obtained by a procedure similar to that carried out in § 4, but it will not be presented here.

The equations (6.5) are of the standard form that arises in quadratic resonance problems and were first obtained by Bretherton (1964) in his resonance study based on a model one-dimensional wave equation. The first example of equations of the form (6.5) in an oceanic context was given by McGoldrick (1965) in his study of capillary–gravity waves. In the limit $B \to 0$ (homogeneous fluid), (6.5) reduce to

$$\left.\begin{aligned} \frac{dA_1}{dT} &= -is\frac{K_3^2 - K_2^2}{K_1^2} A_2 A_3^*, \\ \frac{dA_2}{dT} &= is\frac{K_1^2 - K_3^2}{K_2^2} A_3 A_1, \\ \frac{dA_3}{dT} &= -is\frac{K_2^2 - K_1^2}{K_3^2} A_1 A_2^*. \end{aligned}\right\} \tag{6.7}$$

The coupling coefficients appearing on the right-hand side of (6.7) were first obtained by Kenyon (1964), whereas a certain real form of (6.7) (see §7) was obtained by Longuet-Higgins & Gill (1967) for the case of divergent planetary waves (in which case K_q^2 in the denominator of each term on the right-hand side of (6.7) is replaced by K_q^2+1). Of course in these papers, s is not proportional to γ, but to another parameter that multiplies the nonlinear terms in the governing equations.

7. Analysis of amplitude equations

It is fairly easy to obtain two integrals of (6.5), which correspond to conservation of total energy and generalized or potential enstrophy. To derive the first integral we multiply the first equation in (6.5) by $\cosh K_1 B^{\frac{1}{2}} A_1^*$, the second by $\cosh K_2 B^{\frac{1}{2}} A_2^*$ and the third by $\cosh K_3 B^{\frac{1}{2}} A_3^*$. Then we add these equations to their complex conjugates. The result is, upon using (6.2),

$$\frac{d}{dT}\sum_{q=1}^{3} K_q \sin 2K_q B^{\frac{1}{2}} |A_q|^2 = 0. \tag{7.1}$$

Thus

$$\frac{1}{B^{\frac{1}{2}}}\sum_{q} K_q \sinh 2K_q B^{\frac{1}{2}} |A_q|^2 = \text{constant}, \tag{7.2}$$

which states that the total energy in the triad is conserved. To see that this is the case, we first note that (3.4)–(3.8), (3.11) and (3.13) imply the following energy transfer equation:

$$\frac{\partial}{\partial t}\left(\frac{1}{2}\int_{R_w} E\right) = 0, \tag{7.3}$$

where $E = p_x^{(0)2} + p_y^{(0)2} + B^{-1} p_z^{(0)2}$,

$$\int_{R_w} (\cdot) = \int_0^1 dx \int_y^{y+2\pi/l} dy \int_0^1 dz\,(\cdot), \tag{7.4}$$

and $p^{(0)}$ is periodic in y with period $2\pi/l$. For the single-wave form

$$p^{(0)} = a \sin m\pi x \cos(ly - \omega_m t) \cosh K_m B^{\frac{1}{2}}(z-1),$$

it can be shown from (7.4) that

$$\int_{R_w} E \propto (a^2 K_m \sinh 2K_m B^{\frac{1}{2}})/B^{\frac{1}{2}}. \tag{7.5}$$

Hence (7.3) implies that

$$B^{-\frac{1}{2}} a^2 K_m \sinh 2K_m B^{\frac{1}{2}} = \text{constant},$$

which is the single-wave case of (7.2). For $B \ll 1$ (homogeneous fluid), (7.2) gives the familiar barotropic energy conservation law for a resonant triad [cf. Longuet-Higgins & Gill (1967)]:

$$\sum_{q=1}^{3} K_q^2 |A_q|^2 = \text{constant}.$$

The second conservation law that follows from (6.5) takes the form

$$\frac{1}{B}\sum_{q=1}^{3} K_q^2 \sinh^2 K_q B^{\frac{1}{2}} |A_q|^2 = \text{constant}. \tag{7.6}$$

Since for $B \ll 1$ (7.6) implies that the total *enstrophy* (vorticity squared) is conserved, namely

$$\sum_{q=1}^{3} K_q^4 |A_q|^2 = \text{constant},$$

(7.6) can be said to represent a 'generalized' enstrophy conservation law. Alternatively, (7.6) might be said to represent a 'potential' enstrophy conservation law since, in a stratified fluid of uniform depth, the square of the potential vorticity is conserved in a resonant triad (Richman 1976).

From (6.5) the following 'energy sharing' relations can be easily derived:

$$\frac{K_1 \sinh K_1 B^{\frac{1}{2}}}{P_{23}} \frac{d}{dT} |A_1|^2 = \frac{K_3 \sinh K_3 B^{\frac{1}{2}}}{P_{12}} \frac{d}{dT} |A_3|^2$$
$$= \frac{K_2 \sinh K_2 B^{\frac{1}{2}}}{P_{31}} \frac{d}{dT} |A_2|^2 = 2s \operatorname{Re}\{i A_1 A_2^* A_3\}. \tag{7.7}$$

Suppose there exists a resonant triad with the property that $K_1 < K_2 < K_3$ (figure 4(*a*) is such an example). From (6.2) it can be shown that

$$\operatorname{sgn}(P_{jk}) = \operatorname{sgn}(K_k - K_j); \tag{7.8}$$

thus it follows that $P_{23} > 0$, $P_{12} > 0$ and $P_{31} < 0$. Therefore for this triad, (7.7) implies that waves 1 and 2 are growing in amplitude at the expense of wave 3. If (7.7) is multiplied by (-1) then the opposite situation occurs. In general, however, the energy transfer process is periodic. For a given set of initial conditions (say $A_1(0) = A_{10}$, $A_2(0) = 0$, $A_3(0) = A_{30}$), wave 2 will gradually grow in amplitude, extracting energy from waves 1 and 3; then, after a certain time, wave 2 will start to decay, losing its energy to waves 1 and 3 until the initial conditions are reached; then the process starts all over again. A formula for the period of this energy cycle will be given below.

The amplitude equations (6.5) become particularly simple for the triad

$$(\Omega_{m_1}, l_1, m_1) = (0, 0, 2m)$$

(a steady channel flow),

$$(\Omega_{m_2}, l_2, m_2) = (\Omega, l, m), \quad (\Omega_{m_3}, l_3, m_3) = (\Omega, l, -m).$$

(Note that we have relaxed the condition $m_q > 0$ so that the two interacting waves are distinct.) In this case $K_2 = K_3$ and therefore $P_{23} = 0$ and $P_{31} = -P_{12}$; thus (6.5) implies that $A_1 = \text{constant}$, i.e. the current acts as a catalyst only and does not participate in the energy exchange beteen waves 2 and 3. This triad was first discussed by Longuet-Higgins & Gill (1967) for the case of a homogeneous fluid.

Finally, it is instructive to transform (6.5) into a set of real equations for the moduli and phases of A_q, $q = 1, 2, 3$. If we let

$$A_q(T) = a_q(T) \exp[i\phi_q(T)], \tag{7.9}$$

where a_q and ϕ_q are real functions, then (6.5) gives

$$\left.\begin{aligned} K_1 \sinh K_1 B^{\frac{1}{2}} \dot{a}_1 &= s P_{23} a_2 a_3 \sin\phi, \\ K_2 \sinh K_2 B^{\frac{1}{2}} \dot{a}_2 &= s P_{31} a_3 a_1 \sin\phi, \\ K_3 \sinh K_3 B^{\frac{1}{2}} \dot{a}_3 &= s P_{12} a_1 a_2 \sin\phi, \end{aligned}\right\} \tag{7.10}$$

$$\left.\begin{aligned} a_1 K_1 \sinh K_1 B^{\frac{1}{2}} \dot{\phi}_1 &= -s P_{23} a_2 a_3 \cos\phi, \\ a_2 K_2 \sinh K_2 B^{\frac{1}{2}} \dot{\phi}_2 &= s P_{31} a_3 a_1 \cos\phi, \\ a_3 K_3 \sinh K_3 B^{\frac{1}{2}} \dot{\phi}_3 &= -s P_{12} a_1 a_2 \cos\phi, \end{aligned}\right\} \tag{7.11}$$

where $\dot{} \equiv d/dT$ and $\phi = \phi_2 - \phi_1 - \phi_3$.

Two special cases are of interest. When $\phi = 0$ or π, (7.10) and (7.11) imply that a_q = constant (no energy exchange between the waves) and that $\phi_q \propto T$ + constant. It is fairly easy to show that the constants of integration can be chosen to make $\phi = 0$ or π, even though each ϕ_q varies linearly with T. When $\phi = \frac{1}{2}\pi$ or $\frac{3}{2}\pi$, (7.11) gives ϕ_q = constant and the set (7.10) reduces to the classical gyroscopic equations, which can be integrated in terms of elliptic functions. Note that, when $\phi = \frac{1}{2}\pi$ or $\frac{3}{2}\pi$, the growth rates of the amplitudes are maximized. Therefore this case is of most interest physically. Intermediate cases ($\phi \neq 0, \frac{1}{2}\pi, \pi, \frac{3}{2}\pi$) have been analysed by McGoldrick (1970) and the results are qualitatively similar to the maximum growth rate solutions.

For the sake of completeness we now write down a particular maximum growth rate solution. We take $\phi = \frac{3}{2}\pi$ and a triad such that

$$K_1 < K_2 < K_3. \tag{7.12}$$

Then (7.10) reduces to

$$\left.\begin{aligned} \dot{a}_1 &= -C_{23} a_2 a_3, \\ \dot{a}_2 &= C_{13} a_3 a_1, \\ \dot{a}_3 &= -C_{12} a_1 a_2, \end{aligned}\right\} \tag{7.13}$$

where

$$C_{ij} = \frac{sP_{ij}}{K_q \sinh K_q B^{\frac{1}{2}}}, \quad i \neq j \neq q, \tag{7.14}$$
$$> 0$$

in view of (7.8) and (7.12). Further we suppose that

$$\left.\begin{aligned} a_1(0) &= a_{10} > 0, \\ a_2(0) &= 0, \\ a_3(0) &= a_{30} > 0. \end{aligned}\right\} \tag{7.15}$$

The solution of (7.13) and (7.15) is given by (in the notation of Milne-Thomson 1950)

$$\left.\begin{aligned} a_1(T) &= a_{10}\,\mathrm{dn}\,[a_{10}(C_{12}C_{13})^{\frac{1}{2}} T|m], \\ a_2(T) &= a_{30}(C_{13}/C_{12})^{\frac{1}{2}}\,\mathrm{sn}\,[a_{10}(C_{12}C_{13})^{\frac{1}{2}} T|m], \\ a_3(T) &= a_{30}\,\mathrm{cn}\,[a_{10}(C_{12}C_{13})^{\frac{1}{2}} T|m], \end{aligned}\right\} \tag{7.16}$$

where

$$m = C_{23} a_{30}^2 / C_{12} a_{10}^2 < 1. \tag{7.17}$$

If $m > 1$, the following transformations must be used in (7.16) (Milne-Thomson 1950, p. 19):

$$\begin{aligned} \mathrm{sn}\,(u/m) &= m^{-\frac{1}{2}}\,\mathrm{sn}\,(um^{\frac{1}{2}}|m^{-1}), \\ \mathrm{cn}\,(u/m) &= \mathrm{du}\,(um^{\frac{1}{2}}|m^{-1}), \\ \mathrm{dn}\,(u/m) &= \mathrm{cu}\,(um^{\frac{1}{2}}|m^{-1}). \end{aligned}$$

If $m = 1$, the elliptic functions in (7.16) reduce to hyperbolic functions:

$$\left.\begin{aligned} a_1(T) &= a_{10}\,\mathrm{sech}\,[a_{10}(C_{12}C_{13})^{\frac{1}{2}} T], \\ a_2(T) &= a_{30}(C_{13}/C_{12})^{\frac{1}{2}}\tanh\,[a_{10}(C_{12}C_{13})^{\frac{1}{2}} T], \\ a_3(T) &= a_{30}\,\mathrm{sech}\,[a_{10}(C_{12}C_{13})^{\frac{1}{2}} T]. \end{aligned}\right\} \tag{7.18}$$

The solution (7.16) corresponds to the case where wave 2 continually extracts energy from waves 1 and 3 during the time interval $0 < T < \frac{1}{2}T_d$, where T_d denotes the period

of dn. Then during the time interval $\frac{1}{2}T_d < T < T_d$, the energy transfer is reversed, with waves 1 and 3 continually growing at the expense of wave 2 until the initial conditions are reached. The time over which this energy cycle takes place is

$$T_d = 2K(m)/a_{10}(C_{12}C_{13})^{\frac{1}{2}}, \tag{7.19}$$

where $K(m)$ ($m < 1$) denotes the complete elliptic integral of the first kind. In particular we note that $K(m) \uparrow$ as $m \uparrow$, with $K(1) = \infty$. Thus in the special case $m = 1$ [i.e. solution (7.18)], wave 2 takes an infinitely long time to extract energy from waves 1 and 3.

8. Application to Norwegian Current fluctuations

A large-scale observational study of the Norwegian Current was carried out by the Institut für Meereskunde, Kiel, from 22 July to 5 September 1969. A detailed analysis of the data collected during this study is presented in Horn & Schott (1976). In particular, they found that, at all depths, the current spectra were broadly peaked at around three days; however, they also found a considerable amount of energy at lower frequencies (see figure 5). The region studied is characterized by the following scales:

$$\left.\begin{aligned} f_0 &= 1{\cdot}3 \times 10^{-4}\,\mathrm{s}^{-1}, \\ L &= 40\,\mathrm{m}, \\ H &= 1000\,\mathrm{m}, \\ \alpha &= 1{\cdot}5 \times 10^{-2}, \\ U &= 0{\cdot}3\,\mathrm{m\,s}^{-1}, \\ N^2 &= 6{\cdot}7 \times 10^{-6}\,\mathrm{s}^{-2}, \end{aligned}\right\} \tag{8.1}$$

which in turn give the following values for the non-dimensional parameters used in this paper:

$$\left.\begin{aligned} \delta &= \alpha L/H = 0{\cdot}6, \\ Ro &= U/f_0 L = 0{\cdot}058, \\ \gamma &= Ro/\delta^2 = 0{\cdot}16, \\ B &= \frac{N^2H^2/f_0^2}{L^2} = 0{\cdot}25. \end{aligned}\right\} \tag{8.2}$$

Further, upon using (2.12) it is found that the dimensional wavelength and period of a wave with non-dimensional wavenumber and frequency l and Ω respectively are given by

$$\left.\begin{aligned} \lambda_w &= (251/l)\,\mathrm{km}, \\ T_w &= (0{\cdot}93/\Omega)\,\mathrm{days}. \end{aligned}\right\} \tag{8.3}$$

Figure 6, which is plotted for $\delta = 0{\cdot}6$ and $B = 0{\cdot}25$ [the values in (8.2)], shows an example of a resonant triad that could exist over the Norwegian slope where the above study was made. The triad is characterized by

$$\left.\begin{aligned} (m_1, l_1, \Omega_1) &= (1, 0{\cdot}6, 0{\cdot}1), \\ (m_2, l_2, \Omega_2) &= (2, 4{\cdot}75, 0{\cdot}31), \\ (m_3, l_3, \Omega_3) &= (3, 4{\cdot}15, 0{\cdot}21), \end{aligned}\right\} \tag{8.4}$$

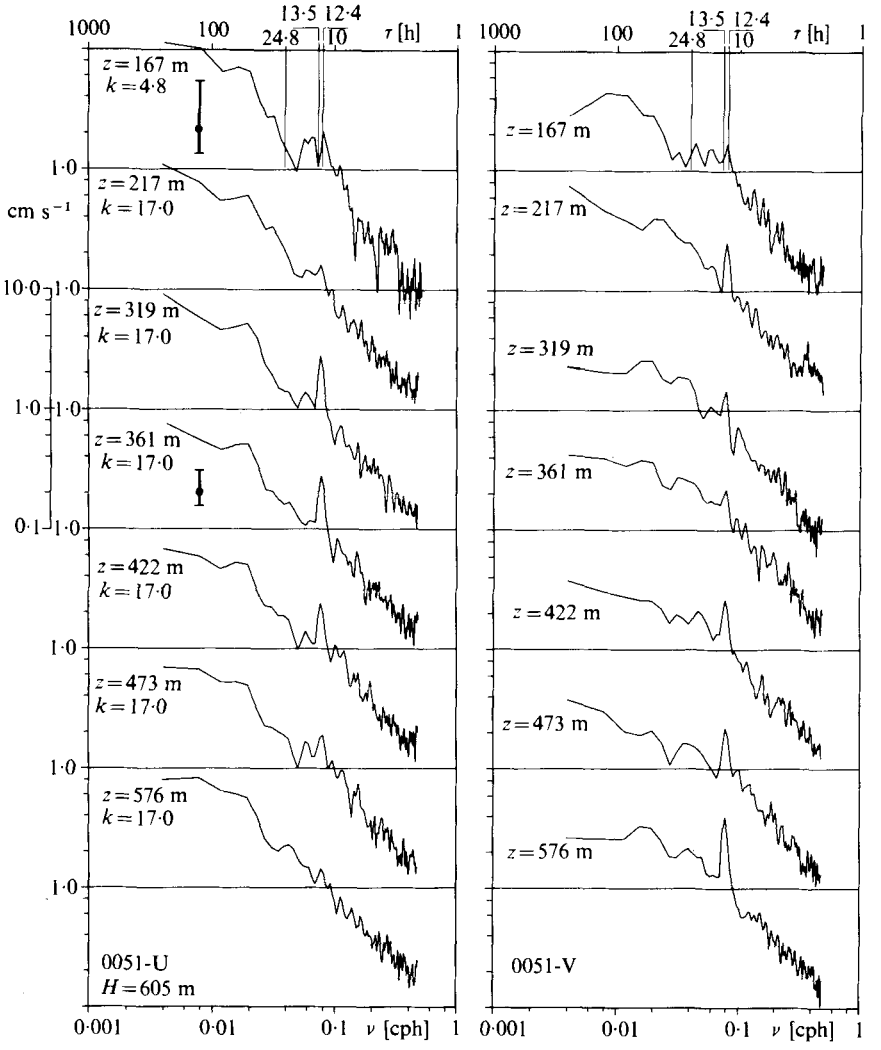

FIGURE 5. Spectra of the longshore (U) and offshore (V) current fluctuations at different depths at a mooring station in the middle of the Norwegian Current, immediately west of Alsesund, Norway. The water depth at this station, which is just beyond the edge of the shelf, is 605 m. The number of degrees of freedom, k, is given, as well as the 95 % confidence bars (from Mysak & Schott 1977).

which is in accordance with the resonance conditions (5.5b). Using (8.3) we find that the corresponding wavelengths and periods are

$$\left.\begin{aligned}(\lambda_{w1}, T_{w1}) &= (418\,\text{km}, 9{\cdot}3\,\text{d})\\ (\lambda_{w2}, T_{w2}) &= (52{\cdot}8\,\text{km}, 3{\cdot}0\,\text{d}).\\ (\lambda_{w3}, T_{w3}) &= (60{\cdot}5\,\text{km}, 4{\cdot}4\,\text{d}).\end{aligned}\right\} \tag{8.5}$$

Thus the interaction is between one long, low-frequency wave and two short, high-frequency waves, the latter having periods near the observed spectral peaks. From (8.4) it follows that

$$K_1 = 3{\cdot}20, \quad K_2 = 7{\cdot}88, \quad K_3 = 10{\cdot}30, \tag{8.6}$$

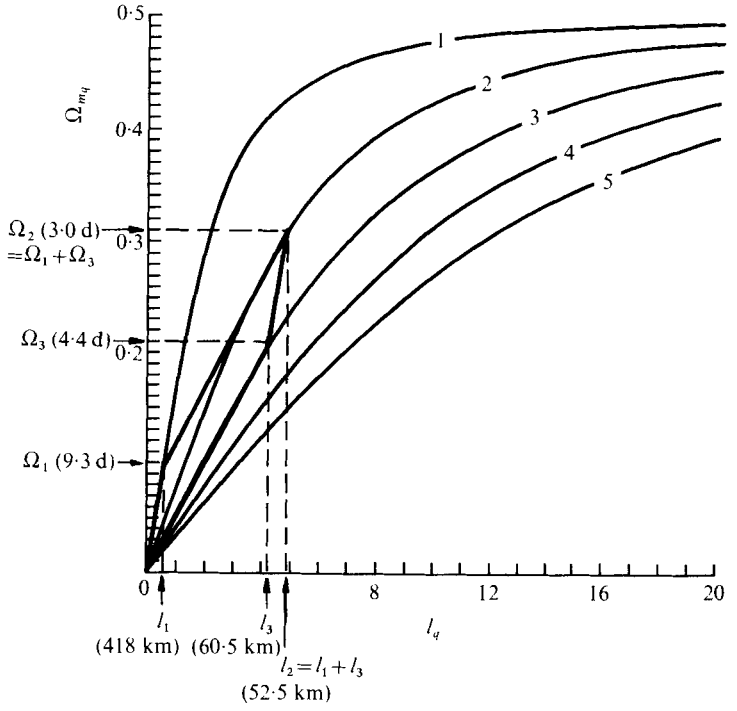

FIGURE 6. Example of a resonant triad that could exist over the Norwegian continental slope. The dispersion curves are plotted for $\delta = 0{\cdot}6$ and $B = 0{\cdot}25$. Ω_{m_q} = frequency, l_q = wavenumber.

so that $K_1 < K_2 < K_3$, in accordance with (7.12). Thus for the initial conditions (7.15), the evolution of the waves' amplitudes is described by (7.16), provided $m < 1$. Using (8.2) and (8.6) in (7.14) we find that $C_{12} = 0{\cdot}55$, $C_{13} = 12{\cdot}1$ and $C_{23} = 1{\cdot}06 \times 10^3$. Thus from (7.17) we see that $m < 1$ provided $a_{30} \ll a_{10}$. In view of the latter inequality, we see from (7.16) that this triad represents the interaction between one 'large' amplitude, long, low-frequency wave and two 'small' amplitude, short, high-frequency waves. Since the observed current spectra at all depths show a considerable amount of energy at periods of four days and longer, as well as the peak at three days, it is quite plausible that resonant interactions between waves of the scales discussed here could take place over the Norwegian continental slope and could serve as a mechanism to transfer energy to larger periods and length scales. However, it should be emphasized that since the spectral peak at around three days is very broad and since there are no spectral peaks at around four and nine days, the example we have given is by no means unique. Indeed, because the spectrum is so broad-banded, a continuum theory of these resonant interactions may in fact be required before we can conclusively establish the existence of this energy process. Work on this extension of the theory is now in progress and will be reported in a future paper. Also, another important question concerns the role of the Norwegian Current itself and whether it may provide an energy source for these resonant waves. In this connexion, it might be worthwhile to study the evolution of a triad in which one wave is unstable on a mean flow. Such a problem was studied by Loesch (1974) for the case for a baroclinic fluid of *uniform* depth.

9. Summary and conclusions

The weak nonlinear interactions between topographic planetary waves in a continuously stratified fluid have been analysed theoretically. For the case of constant stratification and a channel of uniform bottom slope, the following results were obtained.

(i) The lowest-order solution for a single wave travelling down the channel must contain a positive frequency correction (δO) in order to satisfy higher-order terms in the bottom boundary condition. This frequency correction increases monotonically with decreasing stratification (i.e. Burgers number).

(ii) The amplitudes of a triad of such waves containing the frequency correction are governed by the classical gyroscopic equations that arise in most quadratic resonant interaction problems. These amplitudes evolve on the slow dimensional time

$$t = O(1/f_0\delta^2) = O(1/f_0 Ro).$$

In the limit of weak stratification ($B \to 0$), the amplitude equations reduce to the form derived by Longuet-Higgins & Gill (1967).

(iii) For the Norwegian continental slope region, there may exist resonant triads consisting of two short, high-frequency waves and one long, low-frequency wave.

It is suggested that wherever there exist weak quasi-geostrophic motions over a steeply sloping topography [bottom slope $O(10^{-2})$], the possibility of resonant interactions between bottom-trapped waves should be considered. In the recent MODE experiment small-scale, bottom-intensified motions were found over regions of steep topography (Huppert & Bryan 1976). Further, recent numerical spin-down experiments in which the MODE area topography is used show the presence of deep, small-scale eddies (about 50 km across) over regions of steep bottom slopes (Owens & Bretherton 1977). It may be worthwhile to see whether one of these bottom-trapped eddies can be modelled by a resonant triad of the type discussed in this paper.

This paper was written while the author was visiting the National Center for Atmospheric Research (Oceanography Project) during the period February–August 1977. The National Center for Atmospheric Research is sponsored by the National Science Foundation. Throughout the course of this work the author had helpful discussions with Dr F. P. Bretherton, Dr P. Gent, Dr G. Holloway and Dr J. C. McWilliams. The author is also indebted to Mrs Julianna Chow for plotting figures 2–4 and to Ms Karla Nolan for typing the manuscript.

REFERENCES

Bretherton, F. P. 1964 Resonant interactions between waves. The case of discrete oscillations. *J. Fluid Mech.* **20**, 457–479.

Horn, W. & Schott, F. 1976 Measurements of stratification and currents at the Norwegian continental slope. '*Meteor*' *Forsch.-Ergebn* A **18**, 23–62.

Huppert, H. E. & Bryan, K. 1976 Topographically generated eddies. *Deep-Sea Res.* **23**, 655–679.

Kenyon, K. 1964 Non-linear energy transfer in a Rossby-wave spectrum. *Woods Hole Oceanographic Inst., Summer Study Program in Geophysical Fluid Dynamics. Student Lectures*, vol. II, pp. 69–83.

LeBlond, P. H. & Mysak, L. A. 1978 *Waves in the Ocean*. Elsevier.

Loesch, A. Z. 1974 Resonant interactions between unstable and neutral baroclinic waves. *J. Atmos. Sci.* **31**, 1177–1201 (part I), 1202–1217 (part II).

Loesch, A. Z. & Domaracki, A. 1977 Dynamics of N resonantly interacting waves. *J. Atmos. Sci.* **34**, 22–35.

Longuet-Higgins, M. S. & Gill, A. E. 1967 Resonant interactions between planetary waves. *Proc. Roy. Soc.* A **299**, 120–140.

McGoldrick, L. F. 1965 Resonant interactions among capillary-gravity waves. *J. Fluid Mech.* **21**, 305–331.

McGoldrick, L. F. 1970 On Wilton's ripples: a special case of resonant interactions. *J. Fluid Mech.* **42**, 193–200.

Milne-Thomson, L. M. 1950 *Jacobian Elliptic Function Tables*. Dover.

Mysak, L. A. 1977 On the stability of the California Undercurrent off Vancouver Island. *J. Phys. Ocean.* **7**, 904–917.

Mysak, L. A. & Schott, F. 1977 Evidence for baroclinic instability of the Norwegian Current. *J. Geophys. Res.* **82**, 2087–2095.

Newell, A. C. 1969 Rossby wave packet interactions. *J. Fluid Mech.* **35**, 255–271.

Newell, A. C. 1972 The post bifurcation stage of baroclinic instability. *J. Atmos. Sci.* **29**, 64–76.

Owens, W. B. & Bretherton, F. P. 1977 A numerical study of mid-ocean mesoscale eddies. *Deep-Sea Res.* (in press).

Pedlosky, J. 1964 The stability of currents in the atmosphere and ocean: Part I. *J. Atmos. Sci.* **21**, 201–219.

Pedlosky, J. 1975 The amplitude of baroclinic wave triads and mesoscale motion in the ocean. *J. Phys. Ocean.* **5**, 608–614.

Plumb, R. A. 1977 The stability of small amplitude Rossby waves in a channel. *J. Fluid Mech.* **80**, 705–720.

Rhines, P. B. 1970 Edge-, bottom-, and Rossby waves in a rotating stratified fluid. *Geophys. Fluid Dyn.* **1**, 273–307.

Richman, J. G. 1976 Kinematics and energetics of the mesoscale mid-ocean circulation: MODE. Ph.D. thesis, Woods Hole Oceanographic Institution/Massachusetts Institute of Technology.

Smith, P. C. 1976 Baroclinic instability in the Denmark Strait overflow. *J. Phys. Ocean.* **6**, 355–371.

Thompson, R. O. R. Y. & Luyten, J. R. 1976 Evidence for bottom-trapped topographic Rossby waves from single moorings. *Deep-Sea Res.* **23**, 629–635.